Wind and Structures, *Vol. 30, No. 6 (2020) 663-678*
DOI: https://doi.org/10.12989/was.2020.30.6.663

Comparison of semi-active and passive tuned mass damper systems for vibration control of a wind turbine

Eric R. Lalonde[1,3], Kaoshan Dai*[2], Girma Bitsuamlak[3], Wensheng Lu[1] and Zhi Zhao[1]

[1]State Key Laboratory of Disaster Reduction in Civil Engineering, Tongji University, Shanghai, China
[2]Department of Civil Engineering, Sichuan University, Chengdu, China
[3]Department of Civil and Environmental Engineering, University of Western Ontario, London, Canada

(*Received November 21, 2019, Revised March 13, 2020, Accepted April 29, 2020*)

Abstract. Robust semi-active vibration control of wind turbines using tuned mass dampers (TMDs) is a promising technique. This study investigates a 1.5 megawatt wind turbine controlled by eight different types of tuned mass damper systems of equal mass: a passive TMD, a semi-active varying-spring TMD, a semi-active varying-damper TMD, a semi-active varying-damper-and-spring TMD, as well as these four damper systems paired with an additional smaller passive TMD near the mid-point of the tower. The mechanism and controllers for each of these TMD systems are explained, such as employing magnetorheological dampers for the varying-damper TMD cases. The turbine is modelled as a lumped-mass 3D finite element model. The uncontrolled and controlled turbines are subjected to loading and operational cases including service wind loads on operational turbines, seismic loading with service wind on operational turbines, and high-intensity storm wind loads on parked turbines. The displacement and acceleration responses of the tower at the first and second mode shape maxima were used as the performance indicators. Ultimately, it was found that while all the semi-active TMD systems outperformed the passive systems, it was the semi-active varying-damper-and-spring system that was found to be the most effective overall – capable of controlling vibrations about as effectively with only half the mass as a passive TMD. It was also shown that by reducing the mass of the TMD and adding a second smaller TMD below, the vibrations near the mid-point could be greatly reduced at the cost of slightly increased vibrations at the tower top.

Keywords: wind turbine; multiple tuned mass damper; semi-active control; seismic loading; wind loading; case study

1. Introduction

With the ongoing threat of climate change, renewable energy technologies such as wind turbines continue to see increased implementation worldwide. As of 2019, the global installed wind energy capacity was 592 GW (GWEC 2017) and this number continues to grow. The lifespan of wind turbines is traditionally governed by fatigue caused by dynamic wind loading due to the flexibility of the structure. However, there has also been increased erection of wind turbines in areas with high wind or seismic risks, such as parts of the USA, Japan and China, which risks structural failures (Mardfekri and Gardoni 2015, Diaz and Suarez 2014, Chou and Tu 2011). Ensuring long service lives and the safety of wind turbines is critical to keeping their costs low and encouraging further implementation of this technology. Reviews of modern vibration control methods for wind turbines can be found in (Rezaee and Aly 2016, Rahman *et al.* 2015).

A very common structural vibration control method is the tuned mass damper (TMD). The response of the primary structure can be reduced by adding a secondary mass within the structure that can displace relative to the main structure. The TMD is typically connected to the main structure by spring, damper, and/or pendulum systems. The natural frequency of the TMD is tuned by changing the properties of this connection to improve the vibration control effect. TMDs controls include passive, active, and semi-active systems, as shown in Fig. 1. Passive tuned mass dampers (PTMDs) are tuned to a single frequency, typically the natural frequency of the primary structure. PTMDs have been applied to wind turbines in many studies (Sun and Jahangiri 2018, He *et al.* 2017, Lackner and Rotea 2010, Murtagh *et al.* 2008, Argyriadis *et al.* 2004), which have generally concluded that while PTMDs are simple and effective at controlling vibration at their tuned frequency, they tend to have low robustness and lose effectiveness for wideband loading processes. In particular, seismic loading can excite the higher modes of a structure that often are not a concern under wind loading (Zhao *et al.* 2019). If the natural frequency of the primary structure changes over time due to damage or through soil-structure effects, the PTMD will lose effectiveness in turn. Multiple tuned mass dampers (MTMDs) can be used to offset the low robustness of individual PTMDs by tuning each to a different frequency. Additionally, it is often more practical to install multiple small masses within a structure than a single large one, and MTMDs have improved redundancy compared to single TMDs. When applied to wind turbines, passive MTMDs have been shown (Hussan *et al.* 2018, Hussan *et al.* 2017, Zuo *et al.* 2017) to improve the response of the structure when subjected to seismic loading which excites

*Corresponding author, Professor
E-mail: kdai@scu.edu.cn

ISSN: 1226-6116 (Print), 1598-6225 (Online)

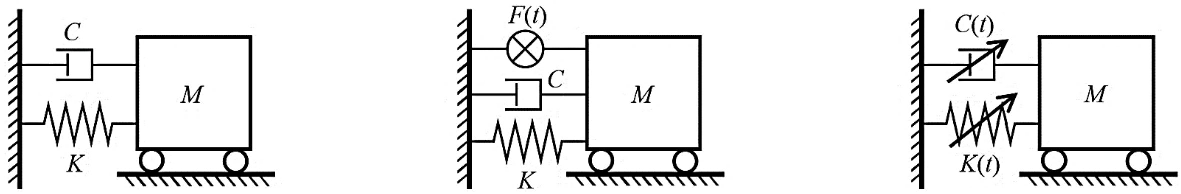

(a) PTMD (b) ATMD (c) STMD

Fig. 1 Simplified models of TMDs connected to main structure

Table 1 Summary of previous studies of wind turbines with semi-active tuned mass dampers

Paper	Turbine structure	STMD location(s)	STMD control method and mechanism*	Does model capture 2nd mode?	2D or 3D model?	Load types	Performance indices
Huang *et al.* (2010)	Floating offshore turbine	Nacelle, blades, platform	Variable stiffness (no mechanism)	No	2D	Wind, wave	Nacelle displacement
Arrigan *et al.* (2011)	Onshore turbine	Nacelle, blades	Variable stiffness (no mechanism)	No	2D	Wind	Nacelle and blade displacement
Martynowicz (2015)	Onshore turbine	Nacelle	Variable damping (numerical and experimental MR damper)	Yes	2D Loading	Harmonic, chirp	Tower top and midpoint displacement
Dinh *et al.* (2016)	Floating offshore turbine	Nacelle, blades, buoy	Variable stiffness (no mechanism)	No	2D	Wind, wave, mooring	Nacelle, blade and buoy displacement
Park *et al.* (2016)	Fixed offshore turbine	Tower top	Variable damping (no mechanism)	Yes	3D	Wind, wave	Fore-aft bending, base moment
Tsouroukdissian *et al.* (2016)	Fixed and floating offshore turbines	Nacelle	Variable damping (no mechanism)	Yes	3D	Wind, wave	Nacelle acceleration
Martynowicz (2016)	Onshore turbine	Nacelle	Variable damping (experimental MR damper)	Yes (experimental)	2D Loading	Harmonic, impulse	Tower top and midpoint displacement
Martynowicz (2017)	Onshore turbine	Nacelle	Variable damping (experimental MR damper)	Yes (experimental)	2D Loading	Harmonic	Tower top and midpoint displacement
Sun (2017)	Fixed offshore turbine	Nacelle	Variable stiffness and damping (no mechanisms)	No	3D	Wind, wave	Nacelle displacement, base rotation
Hemmati *et al.* (2018)	Fixed offshore turbine	Nacelle	Variable stiffness and damping (no mechanisms)	Yes	2D	Wind, wave, seismic	Nacelle displacement, base shear and moment
Park *et al.* (2019)	Fixed and floating offshore turbines	Tower top	Variable damping (numerical MR damper)	Yes	3D	Wind, wave	Nacelle displacement, base moment

*Here, the term "mechanism" refers to whether the paper presents a mechanical explanation of how the stiffness and/or damping of the TMD is varied, such as modelling a variable damping system using a magnetorheological damper

the higher modes of the structure. However, this may come at the cost of reduced vibration control under service wind loading compared to a single PTMD.

Active tuned mass dampers (ATMDs) include actuators that apply an active force to the TMD mass to improve the vibration control effect. There have been multiple studies of ATMDs used in wind turbines (Brodersen *et al.* 2017, Stewart 2012, Lackner and Rotea 2011) which all have shown a strong capability for vibration control, however ATMDs are often limited by the large electrical cost of running the actuators as well as lower reliability compared to PTMDs.

Semi-active tuned mass dampers (STMDs) combine the benefits of passive and active systems by modifying their stiffness or damping values in real-time to improve their vibration control capabilities. In traditional structures, STMDs have been shown to be about as effective as ATMDs, but with better reliability and reduced electrical costs (Kaveh *et al.* 2015, Sun *et al.* 2014, Eason *et al.* 2013, Chung *et al.* 2013, Esteki *et al.* 2011; Owji *et al.* 2011, Chey *et al.* 2009, Nagarajaiah and Sonmez 2007, Yang *et al.* 2002, Pinkaew and Fujino 2001, Ricciardelli *et al.* 2000,

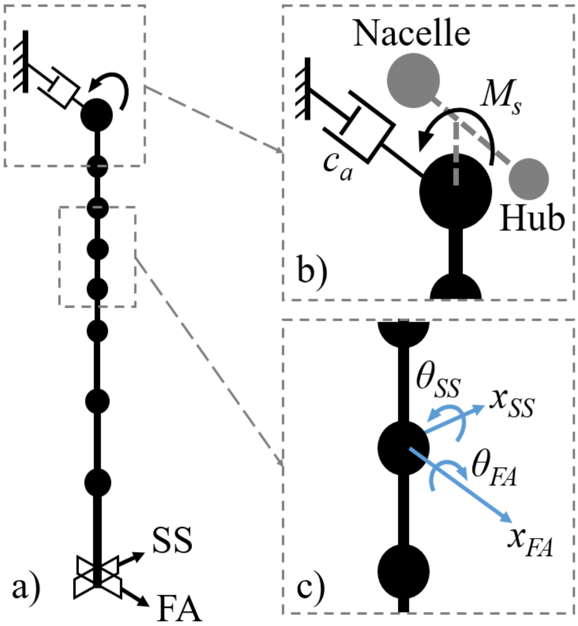

Fig. 2 (a) The 32-DOF FEM turbine model (b) Eccentricity moment and aerodynamic damping of the top node (c) DOFs of a single lumped-mass node

Hrovat *et al.* 1983). There are two main methods of controlling an STMD: by modifying the TMD stiffness in real-time to change the tuning, increasing its robustness; or modifying the damping in real-time to increase the amount of energy absorbed by the TMD. While both techniques have been shown to improve effectiveness compared to PTMDs, some studies (Nagarajaiah 2009) recommend employing the variable stiffness dampers due to the improved robustness and the ability to tune the damper to the structural loading rather the natural frequency of the structure. Some studies also employ both variable stiffness and damping simultaneously to control their STMDs (Sun and Nagarajaiah 2013). There are several instances of single and multiple STMDs with various control methods being employed in wind turbines, all of which conclude that the improved robustness of the STMDs makes them more effective than traditional PTMDs - these papers are summarized in Table 1.

These previous studies make it clear that STMDs can be effective at controlling vibrations in wind turbines. However, Table 1 shows there exists limitations in the previous research: they frequently test a smaller number of load cases using models that simplify the tower as a single beam, which does not give the second mode response full consideration. With a few exceptions (Park *et al.* 2019), the effectiveness of the proposed STMD is only compared to an equivalent PTMD, not to other STMDs. Frequently these studies do not approach the design of the TMDs from a pragmatic perspective: the physical systems used to allow for varying stiffness or damping are not modelled but merely assumed, which may result in the semi-active behaviour of these models being unrealistically precise. Additionally, many studies place the TMD in the wind turbine nacelle without acknowledging that there is limited space there for such a system in modern wind turbine designs. A practical TMD design must allow workers to climb the tower to maintain the turbine, and if placed within the nacelle it must not interfere with the generator and other internal systems.

This paper aims to build upon the previous literature by studying the effectiveness of various passive and semi-active single and multiple TMD systems with a focus on addressing the gaps in previous research by comparing a wide array of equivalent, fully-detailed TMDs. It compares a 3D turbine model equipped with eight equivalent-mass TMD systems – a passive TMD, an STMD with a varying-spring system, an STMD with a varying-damper system, an STMD with a varying-damper-and-spring system, as well as MTMD configurations of these four – to an uncontrolled turbine under service wind loads, high intensity wind loads, and seismic loads with service wind. Firstly, the design of the wind turbine, the loading cases, and the TMD models is presented. The effectiveness of the various TMD systems is compared by examining the response of the turbines at the maxima of the first two modes. Finally, a pragmatic TMD for modern wind turbines is proposed.

2. Test methodology

2.1 Turbine model

The turbine model used in this study was a lumped-mass, 32-degree-of-freedom (DOF), 3D turbine finite element model (FEM) built in MATLAB. The model consisted of a tower made of beam elements with a fixed base, which allowed for multiple modes to be analyzed in both the fore-aft (FA) and side-side (SS) directions. The turbine nacelle and blades were modelled as a lumped mass at the top of the tower, a simplification applied in many numerical turbine studies (Zhang *et al.* 2019, Hussan *et al.* 2017, Dai *et al.* 2017a, Brodersen *et al.* 2016, Dai *et al.* 2015, Prowell *et al.* 2009). MATLAB was employed here to accommodate possible future tests.

The FEM model used eight prismatic beam elements in the tower above a fixed foundation, as shown in Fig. 2, each of which had eight DOFs which corresponded to the lateral displacements and rotations at the ends of the beams. Each lumped-mass node was thus capable of displacement and rotation in the FA and SS directions (x_{FA}, θ_{FA}, x_{SS} and θ_{SS} respectively). Axial deformation and torsion were not considered in this study. The hub and nacelle masses were lumped into the top node and a moment was applied to account for their eccentricity. c_a is the aerodynamic damping dashpot and M_s is the static moment caused by the hub and nacelle eccentricity, which are quantified below.

Eqs. (1) - (2) were used to calculate the stiffness and distributed mass element matrices in this model (Reddy 1993). Here $[K_e]$ and $[M_e]$ are the symmetrical stiffness and mass element matrices respectively, L_e is the element length, EI_e is the flexural rigidity of the element, and LD_e is its linear density. Note that since turbine towers are built from circular hollow steel sections, the simplified mass, stiffness and modal properties are the same in the FA and SS directions.

Table 2 Turbine tower properties

Tower Section	Element Length (m) L_e	Flexural Rigidity (Nm^2) EI_e	Linear Density (kg/m) LD_e	Tower Section	Element Length (m) L_e	Flexural Rigidity (Nm^2) EI_e	Linear Density (kg/m) LD_e
1 (TOP)	5.60	2.22E+10	739	5	5.40	5.15E+10	1043
2	5.46	2.73E+10	792	6	9.04	6.68E+10	1248
3	5.44	3.31E+10	844	7	11.76	8.19E+10	1529
4	5.42	3.96E+10	896	8 (BOTTOM)	13.61	1.12E+11	2084

Table 3 Modal analysis of simplified FEM (MATLAB), SAP 2000, FAST models and field measurements

	1st FA Freq. rad/s (Hz)	2nd FA Freq. rad/s (Hz)	1st SS Freq. rad/s (Hz)	2nd SS Freq. rad/s (Hz)
Simplified FEM Model	3.503 (0.558)	31.6 (5.03)	3.503 (0.558)	31.6 (5.03)
SAP 2000 Model	3.501 (0.557)	31.0 (4.93)	3.501 (0.557)	31.0 (4.93)
% Difference vs Simplified	0.057%	1.9%	0.057%	1.9%
FAST Model	3.21 (0.511)	30.3 (4.82)	3.21 (0.511)	30.3 (4.82)
% Difference vs Simplified	8.3%	4.1%	8.3%	4.1%
Field Measurements	3.08 (0.490)	24.2 (3.85)	3.02 (0.481)	25.6 (3.85)
% Difference vs Simplified	12.1%	23.5%	13.8%	18.9%

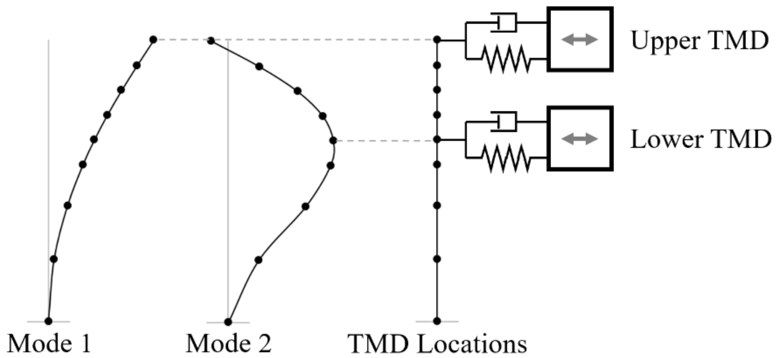

Fig. 3 Mode shapes and resulting TMD locations

$$[K_e] = \frac{2EI_e}{L_e^3} * \begin{bmatrix} 6 & & & & & & & \\ -3L_e & 2L_e^2 & & & & & & \\ 0 & 0 & 6 & & & \cdots & & \\ 0 & 0 & -3L_e & 2L_e^2 & & & & \\ -6 & 3L_e & 0 & 0 & 6 & & & \\ -3L_e & L_e^2 & 0 & 0 & 3L_e & 2L_e^2 & & \\ 0 & 0 & -6 & 3L_e & 0 & 0 & 6 & \\ 0 & 0 & -3L_e & L_e^2 & 0 & 0 & 3L_e & 2L_e^2 \end{bmatrix} \tag{1}$$

$$[M_e] = \frac{LD_e * L_e}{210} * \begin{bmatrix} 78 & & & & & & & \\ 11L_e & 2L_e^2 & & & & & & \\ 0 & 0 & 78 & & & \cdots & & \\ 0 & 0 & 11L_e & 2L_e^2 & & & & \\ 27 & 7.5L_e & 0 & 0 & 78 & & & \\ -7.5L_e & -1.5L_e^2 & 0 & 0 & -11L_e & 2L_e^2 & & \\ 0 & 0 & 27 & 7.5L_e & 0 & 0 & 78 & \\ 0 & 0 & -7.5L_e & -1.5L_e^2 & 0 & 0 & -11L_e & 2L_e^2 \end{bmatrix} \tag{2}$$

Previous research has shown that when the aerodynamic damping provided by the rotation of the blades is considered, operational turbines have a damping ratio of approximately 5% in the FA direction and a value of 0.5% (Katsanos *et al.* 2016) to 1% (Mardfekri and Gardoni 2015) in the SS direction – the latter value was used in this study. This behavior was captured here using Rayleigh damping based on the first two FA natural frequencies and a 1% structural damping ratio. The additional aerodynamic damping was simulated using a linear damper attached to the top of the turbine and oriented in the FA direction, a technique suggested by Valamanesh and Myers (2014). The damping coefficient for this damper was calculated using Eq. (3) based on the assumption that the first mode will govern the response at the top of the tower. Here m_{m1} is the first modal mass; ω_1 is the first natural frequency in the FA direction; and ξ_a is the aerodynamic damping ratio of 4% (this plus the 1% structural damping reached the target value of 5%). When the turbine was in the parked condition, c_a was set to zero.

$$c_a = 2 * m_{\mathrm{m1}} * \omega_1 * \xi_a \tag{3}$$

The turbine used in this study was a standard 1.5 MW three-blade horizontal axis wind turbine with a hub height of 65 m (Zhang *et al.* 2019, Zhao *et al.* 2019, Dai *et al.*

Table 4 List of applied load cases

Load Case	Main Loading Direction	Operation State	Number of Time Histories
SW – 10m/s	FA	Operational	10
SW – 15m/s	FA	Operational	10
SW – 20m/s	FA	Operational	10
SW – 25m/s	FA	Operational	10
HIW – 35m/s	SS	Parked	10
HIW – 40m/s	SS	Parked	10
HIW – 45m/s	SS	Parked	10
HIW – 50m/s	SS	Parked	10
HIW – 55m/s	SS	Parked	10
HIW – 60m/s	SS	Parked	10
EQ1 with SW – 10m/s	FA, SS, and FA+SS	Operational	3
EQ2 with SW – 10m/s	FA, SS, and FA+SS	Operational	3
EQ3 with SW – 10m/s	FA, SS, and FA+SS	Operational	3
EQ4 with SW – 10m/s	FA, SS, and FA+SS	Operational	3
EQ5 with SW – 10m/s	FA, SS, and FA+SS	Operational	3
EQ6 with SW – 10m/s	FA, SS, and FA+SS	Operational	3
EQ7 with SW – 10m/s	FA, SS, and FA+SS	Operational	3

Table 5 Summary of IEC wind field parameters for 1.5 MW wind turbine

Parameter	Normal wind model (SW)	Extreme turbulent wind model (HIW)
Turbulence intensity I_{ref}	0.16	
Turbulence standard deviation σ_1	$\sigma_1 = I_{ref}(0.75V_{hub} + 5.6)$	$\sigma_1 = 0.11V_{hub}$
Wind profile $V(z)$, where z is height in meters and $z_{hub} = 65$ m	$V(z) = V_{hub}\left({}^{z}/_{z_{hub}}\right)^{0.2}$	$V(z) = V_{hub}\left({}^{z}/_{z_{hub}}\right)^{0.11}$
Equivalent 10 m design wind speed V_{10}	$V_{10} = 0.688V_{hub}$	$V_{10} = 0.814V_{hub}$
Spectrum $S(f)$	$S(f) = 0.05{\sigma_1}^2({}^{42}/_{V_{hub}})^{-\frac{2}{3}}f^{-\frac{5}{3}}$	

2017a, Sadowski *et al.* 2017). Table 2 lists the tower properties used in Eqs. (1) - (2). As shown in Fig. 2, the hub was modelled as a 16.83 t lumped mass 1.5 m above and 2.5 m in front of the center of the tower top, and the nacelle was modelled as a 60 t mass 1.5 m above and 1m behind. Sadowski *et al.* (2017) found the first and second modal mass contributions for this turbine to be 64% and 18% respectively, thus $m_{m1} \approx 100$ t and $m_{m2} \approx 28$ t. The damping coefficient of the aerodynamic dashpot was calculated using Eq. (3) to be 28000 Ns/m. Modal analysis identified the maximum of the first mode shape at the top of the tower (at a height of 61.7 m) and the maximum of the second mode shape at the fifth node from the top (at a height of 39.8 m), which were chosen as the installation locations for the upper and lower TMDs (see Fig. 3).

This simplified FEM model of the uncontrolled turbine was verified by comparing the first two natural frequencies in the FA and SS directions to an identical 8-element model built in SAP 2000, as well as a more detailed FEM model in the open-source turbine modelling software FAST (Jonkman 2018). It was also verified against field measurements of the operational turbine which provides the basis for the test turbine (Dai *et al.* 2017b). Table 3 shows that the first and second modes in the FA and SS directions were almost identical between MATLAB and SAP 2000 model, with an increased error compared to the FAST and field measurements due to simplifications present in the 8-element turbine model.

2.2 Applied load cases

Three general loading conditions were considered in this study: multi-directional earthquake (EQ) loading combined with service wind loads to an operational wind turbine, high-intensity wind (HIW) loads applied in the SS direction to a parked wind turbine (which has been shown to be the worst wind loading case (Zhang *et al.* 2019, Wang *et al.* 2013), and service wind (SW) loads applied in the FA direction to an operational turbine. Table 4 summarizes the time histories used in this testing, with full explanations of each found in the following sections. The speeds following the wind load cases refer to the mean hub wind speed. Test durations were chosen such that the test lengths of all cases were the same, thus an overall duration of 85 s was used. In seismic cases the ground motion was applied 15 s into the test. A total of 40 SW, 60 HIW, and 21 EQ load cases were applied to the uncontrolled turbine as well as the eight TMD types for a total of 1089 trials.

2.2.1 Wind loading

Both 50-year HIW loads and SW loads were generated using the following technique, which is described in more detail in Zhao *et al.* (2019). First, wind fields were generated in TurbSim (Kelly and Jonkman 2012) using random seeds, with parameters selected according to IEC guidelines (IEC 2005) using the normal wind and extreme turbulent wind models. Table 5 summarizes the parameters

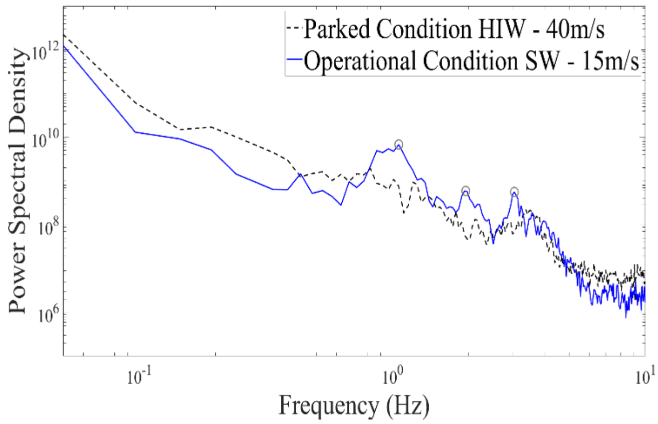

Fig. 4 Power spectrum density of concentrated FA blade load time histories

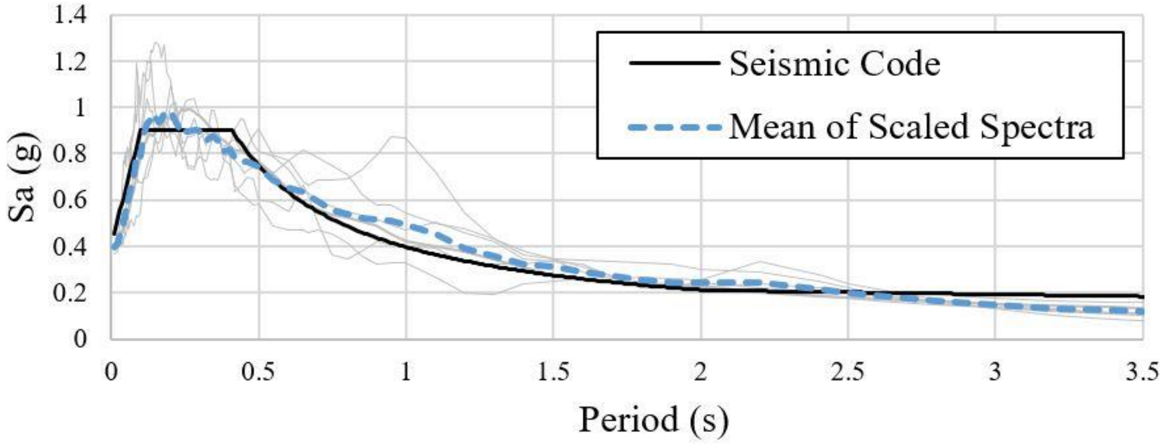

Fig. 5 Mean of seven scaled seismic record response spectra compared to the seismic code requirement for rare earthquakes

and equations, which are based on the mean hub wind speeds (V_{hub}) listed in Table 4. TurbSim then uses the Sandia method (Veers 1988) to generate the wind fields. Secondly, these newly generated wind fields were applied to the uncontrolled test turbine in FAST (Jonkman 2018), which uses the blade element momentum (BEM) theory (Glauert 1935) to calculate the resulting blade loads on the tower. The time history of these blade loads were applied to the FEM model of the controlled wind turbine during testing. This TurbSim-FAST-FEM process to model blade loads has been applied in several other studies (Mo *et al.* 2017, Asareh *et al.* 2016, Mardfekri and Gardoni 2015). Tower and nacelle loads were applied as concentrated loads at the appropriate DOF, which were likewise generated using FAST.

The SW conditions ranged from a mean hub wind velocity of 10 m/s to 25 m/s, and the HIW conditions ranged from 35 m/s to 60 m/s. Since this testing was limited to elastic turbine response, the maximum design wind speed of 60 m/s for the test turbine was not exceeded.

Fig. 4 shows the power spectrum density of the concentrated FA blade loads calculated in FAST under representative operational and parked conditions. The peaks at 1, 2 and 3 Hz in the operational condition due to rotation of the blades are highlighted, which disappear in the parked condition.

2.2.2 Seismic loading

As suggested by the Chinese seismic design code (MHURD 2010), seven ground motion records were scaled such that their mean spectra matched the 5%-damping design response spectrum for rare earthquakes shown in Fig. 5. Table 6 lists the chosen ground motion records and scaling factors, which were selected from the PEER database (Ancheta *et al.* 2013). Both the N-S and E-W components were applied during testing, where it was randomly selected whether the N-S or E-W would correspond to the FA direction of the turbine. Seismic loading was applied to operational turbines, which were simultaneously subjected to 10 m/s SW loads.

2.3 TMD models

TMDs reduce vibrations in structures by applying a restoring force in response to movement, as shown in Fig. 6 where a TMD (m_2) applies forces to main structure (m_1) via a damper (F_D) and a spring (F_S). Eqs. (5) - (6) show the equations of motion of the main structure and the TMD for the 2-DOF case shown in Fig. 6. Here m_1, c_1, k_1 are the mass, damping and stiffness of the main structure; m_2 is the mass of the TMD; x_1, $\dot{x}_1$, $\ddot{x}_1$ are the displacement, velocity and acceleration of the main structure; x_2, $\dot{x}_2$, $\ddot{x}_2$ are the displacement, velocity and acceleration of the TMD;

Table 6 Selected scaled ground motion records

No.	Earthquake name and station	Scaling factor
1	Imperial Valley-02 (1940) – El Centro Station #9	1.55
2	Imperial Valley-06 (1979) – El Centro Array #12	1.53
3	Superstition Hills-02 (1987) - Westmorland Fire Station	1.38
4	Manjil Iran (1990) - Abbar	0.51
5	Chi-Chi Taiwan (1999) – TCU122	1.97
6	Iwate Japan (2008) – IWT010	3.17
7	Darfield New Zealand (2010) – Christchurch Cashmere HS	0.86

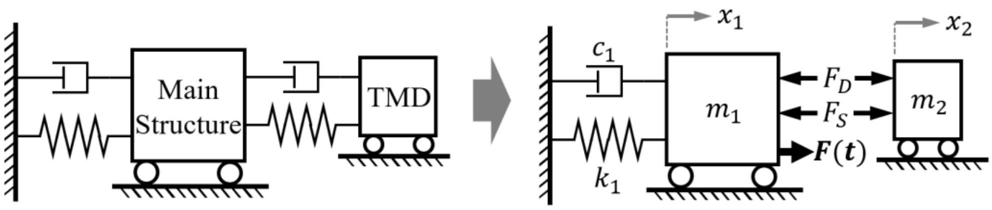

Fig. 6 Approximating TMD restoring forces applied to main structure in 2-DOF case as F_D and F_S

Table 7 Summary of test cases (see Fig. 3 for TMD locations)

	Upper TMD				Lower TMD		
Test case:	TMD mass	Modal mass ratio	Damper controller	Spring controller	TMD mass	Modal mass ratio	Spring and damper controllers
NoTMD	0	-	-		0	-	-
1PTMD	M	3%	Passive [2.3.2]	Passive [2.3.3]	0	-	-
1VarS	M	3%	Passive [2.3.2]	Semi-active [2.3.5]	0	-	-
1VarD	M	3%	Semi-active [2.3.4]	Passive [2.3.3]	0	-	-
1VDVS	M	3%	Semi-active [2.3.4]	Semi-active [2.3.5]	0	-	-
2PTMD	0.9*M	2.7%	Passive	Passive	0.1*M	1.1%	Passive
2VarS	0.9*M	2.7%	Passive	Semi-active	0.1*M	1.1%	Passive
2VarD	0.9*M	2.7%	Semi-active	Passive	0.1*M	1.1%	Passive
2VDVS	0.9*M	2.7%	Semi-active	Semi-active	0.1*M	1.1%	Passive

$F(t)$ is the applied force from wind and/or seismic loading; F_D is the damper force which is primarily a function of $(\dot{x}_1 - \dot{x}_2)$; and F_S is the spring force which is primarily a function of $(x_1 - x_2)$.

$$m_1\ddot{x}_1 + c_1\dot{x}_1 + k_1x_1 = F - F_D - F_S \tag{5}$$

$$m_2\ddot{x}_2 = F_D + F_S \tag{6}$$

In this study, the results of the turbines equipped with eight different TMD systems were compared to the uncontrolled turbine. This paper placed the upper TMD within the top section of the turbine tower. Since it could not rotate with the nacelle, a 2D TMD capable of displacing in both the FA and SS directions was used. In the FEM model, the resulting forces from the upper TMD were applied to the lateral FA and SS DOFs at the top node of the tower. In the MTMD cases, the lower TMD was placed at the fifth node of the model from the top [see Fig. 3], which was approximately 40m above the ground. This location represents the maximum response of the second mode shape of the tower and has been found to be a failure point of turbine towers under seismic loading (Zhao *et al.* 2019). All eight damper systems used the same collective modal mass ratio of 3%. Damper optimization was performed using the same performance indices analyzed in Section 3 of this paper. Additionally, a maximum TMD stroke limit of ±1 m was placed on all TMDs, which was assumed as a reasonable upper limit due to the 3 m interior diameter of the top section of the turbine tower. The specifics of the eight TMDs, their controllers, and how they calculate F_D and F_S are explained in the following sections.

2.3.1 Summary of test cases

Table 7 below summarizes the eight TMD cases studied for each load case. The tests consisted of the uncontrolled turbine, four single-TMD cases (one passive and three semi-active) and four MTMD cases consisting of a large upper TMD and a smaller lower TMD. Each TMD case is a unique combination of the damper and spring controllers detailed in Sections 2.3.2-2.3.5. For example, the single-TMD varying-damper-and-spring (1VDVS) case used the varying-damper and varying-spring controllers (with slight provisions made for the additional stiffness added by the varying-damper [see Sections 2.3.4 and 2.3.5]) in the upper TMD and did not include a lower TMD.

In the MTMD cases the upper TMD was either passive

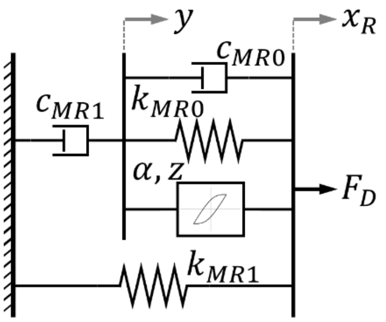

Fig. 7 Modified Bouc-Wen model – a numerical approximation of an MR damper

or semi-active, however the lower TMD was always passive as preliminary testing found that an impractically small time step during simulations was required to guarantee stability, while not resulting in significant response improvement. In Table 7, M is the mass of the single TMD cases, which was equal to 3% of the first modal mass of the turbine. The combined mass of the MTMD cases were made equal to the mass of the single TMD cases so that the effectiveness of the two methods could be roughly compared, and a 90-10 split between upper and lower masses was found to be near optimal – this results in a 2.7% mass ratio compared to the first mode for the upper TMD and a 1.1% mass ratio compared to the second mode for the lower TMD. The optimized parameters for the TMD controllers are summarized in Section 2.3.6.

2.3.2 Passive damper design

The passive damper controller was employed in the PTMD and VarS cases, and was tuned following the Den Hartog guidelines presented in Connor (2002). Eqs. (7) - (10) show the calculation procedure for the damper force (F_D) based on the modal mass ratio (μ) listed in Table 7. Here, Q_j is the optimal ratio between the natural frequency of the TMD and modal frequency of the turbine, ξ_j is the damping coefficient, m_{mj} is the modal mass, ω_{mj} is the modal frequency, c_j is the damping coefficient, and $(\dot{x}_1 - \dot{x}_2)$ is the relative velocity of the TMD [Fig. 6]. j = 1 refers to the first mode and j = 2 refers to the second mode; recall that the upper TMD is always tuned to the first mode and the lower TMD is tuned to the second.

$$\xi_j = \sqrt{\frac{\mu\left(3-\sqrt{0.5\mu}\right)}{8(1+\mu)(1-0.5\mu)}} \tag{7}$$

$$Q_j = 1 - 1.2\mu \tag{8}$$

$$c_j = 2\left(\mu * m_{mj}\right)\left(Q_j * \omega_{mj}\right)\xi_j \tag{9}$$

$$F_D = c_j * (\dot{x}_1 - \dot{x}_2) \tag{10}$$

2.3.3 Passive spring design

The passive spring controller was employed in the PTMD and VarD cases, using the same guidelines and nomenclature from Section 2.3.2. Eqs. (11) - (12) show the calculation procedure for the spring force (F_S) based on the modal mass ratio (μ) listed in Table 7. Here, k_j is the stiffness, and $(x_1 - x_2)$ is the relative displacement of the TMD (Fig. 6).

$$k_j = \left(\mu * m_{mj}\right)\left(Q_j * \omega_{mj}\right)^2 \tag{11}$$

$$F_S = k_j * (x_1 - x_2) \tag{12}$$

2.3.4 Semi-active varying-damper controller using an MR damper

The semi-active varying-damper controller was employed in the VarD and VDVS cases, and consisted of a magnetorheological (MR) damper – MR dampers are filled with a fluid whose apparent viscosity changes when subjected to an electric current, allowing their properties to be controlled in real time. MR dampers have been frequently studied for turbine vibration control (Martynowicz 2017, Martynowicz 2016, Caterino *et al.* 2016, Martynowicz 2015, Caterino *et al.* 2014, Caterino 2014). These dampers can be numerically simulated using the Modified Bouc-Wen (MBW) model (Talatahari *et al.* 2012, Caterino *et al.* 2011, Spencer *et al.* 2004) shown in Fig. 7. Though there have been criticisms of the accuracy of the MBW model for modelling very powerful dampers (Chae *et al.* 2012), it should be accurate for the small damper modelled in these tests. Eqs. (13) - (19) list the calculations used for determining the damper force (F_D), where u is the efficient voltage; v is the applied voltage; z is the hysteretic displacement; x_R is the relative displacement of the MR damper to the turbine (equal to x_1 - x_2 from Eq. (5)), y, k_{MR0}, k_{MR1}, c_{MR0}, c_{MR1} are the displacement, stiffnesses, and damping shown in Fig. 7 and α_a, α_b, c_{MR0a}, c_{MR0b}, c_{MR1a}, c_{MR1b}, k_{MR0}, k_{MR1}, x_{R0}, γ, β, A, n, η are the fourteen parameters of the MBW model for a given MR damper which are derived from experimental testing. This paper reused the MBW model properties given in Table 1 of Li *et al.* (2017) for a 2.4 kN RD-8041-1 MR damper. The backwards difference method was used to solve the differentials of z and y.

$$F_D = [\alpha * z + c_{MR0} * (\dot{x}_R - \dot{y}) + k_{MR0} * (x_R - y) + k_{MR1} * (x_R - x_{R0})] \tag{13}$$

$$\dot{z} = -\gamma * |\dot{x}_R - \dot{y}| * z * |z|^{n-1} - \beta * (\dot{x}_R - \dot{y}) * |z|^n + A * (\dot{x}_R - \dot{y}) \tag{14}$$

$$\dot{y} = \frac{1}{(c_{MR0} + c_{MR1})} * [\alpha * z + c_{MR0} * \dot{x}_R + k_{MR0} * (x_R - y)] \tag{15}$$

$$\alpha(u) = \alpha_a + \alpha_b * u \tag{16}$$

$$c_{MR0}(u) = c_{MR0a} + c_{MR0b} * u \tag{17}$$

$$c_{MR1}(u) = c_{MR1a} + c_{MR1b} * u \tag{18}$$

$$\dot{u} = -\eta * (u - v) \tag{19}$$

Martynowicz (2016) studied several types of varying-damper STMD controllers and found that a modified ground-hook (MGH) controller was highly effective and simple to implement, thus it was applied here [Eq. (20)]. A simplified explanation of the controller is that it maximizes resistance force by applying the maximum voltage to the MR damper when the structure moves away from its neutral position and minimizes resistance force by applying the minimum voltage when the structure returns to its neutral position. The MGH controller can be displacement-based or velocity-based, each of which have been shown to have their own advantages (Park *et al.* 2019), but the displacement-based method was used here as that was the method tested by Martynowicz (2016). For thoroughness, a more complex LQR controller (Hrovat *et al.* 1983) for the MR damper was also tested, but the MGH controller was found to be more effective. An artificial 10 ms delay was added to the VarD system between calculating and applying the desired voltage to more closely simulate the physical system (Caterino *et al.* 2013).

$$v_{MR} = \begin{cases} v_{max}, & x_1 * F_D \geq 0 \\ v_{min}, & x_1 * F_D < 0 \end{cases} \tag{20}$$

Note that as opposed to a linear damper, the MBW model includes a varying stiffness component [Eq. (13)]. Some previous research has shown that the stiffness component contributes very little to the overall resistance force (Caterino *et al.* 2011) – in this study the optimized MR damper temporarily increased the stiffness of the TMD by a maximum of 2%. Thus this additional stiffness was ignored in the VarD case where the passive spring system cannot easily account for this increase in stiffness, but was accounted for in the VDVS case [see Section 2.3.5] using k_{MR}: the equivalent MR stiffness at a given time step which was calculated using Eq. (21).

$$k_{MR} = \frac{\left(k_{MR0} * (x_R - y) + k_{MR1} * (x_R - x_{R0})\right)}{(x_R - x_{R0})} \tag{21}$$

2.3.5 Semi-active varying-spring controller using SAIVS system

The semi-active varying-stiffness controller was used in the VarS and VDVS cases, and employs the SAIVS system (Sun and Nagarajaiah 2013, Nagarajaiah 2009, Nagarajaiah 2007) to modify the stiffness of the TMD in real-time. This system uses an actuator to adjust an array of four springs to actively change the equivalent stiffness of the TMD. Eq. (22) shows the equation for the equivalent stiffness as a function of the actuator displacement d in meters which could range from 0.0 (the minimum stiffness) to 0.3 (the maximum stiffness). It was found that the total stiffness range required could be achieved when k_{SAIVS} was equal to 160 kN/m.

$$k_2(d) = k_{SAIVS} * \cos^2\left[\frac{\pi}{2} * \sin\frac{\pi(0.3 - d)}{0.6}\right] \tag{22}$$

The SAIVS was tuned by using a short-term Fourier transform (STFT) to determine the dominant frequency of the recent lateral acceleration of the top of the turbine tower and tuned the TMD to match that frequency: a widely-used technique (Park *et al.* 2019; Hemmati *et al.* 2018, Sun 2017, Dinh *et al.* 2016, Arrigan *et al.* 2011, Huang *et al.* 2010). Some studies tune the varying-spring to the dominant frequency of the displacement of the turbine tower (Sun 2017), but acceleration was used in this study due to the improved practicality as in reality an accelerometer may be used to easily capture the acceleration response. This STFT controller applied a Hann window function [Eq. (23)] to a segment of the previous top lateral acceleration response to extract the dominant frequency, which the TMD was then tuned to. If this target frequency was outside of the range of the SAIVS system, the TMD was instead tuned to the main structural frequency using Eqs. (11) - (12). In either case, the target stiffness at the given time step was reduced by k_{MR} [Eq. (21)]: the stiffness added by the varying-damper system. k_{MR} = 0 in all configurations but the VDVS cases. A tight allowable frequency band was found to be the overall most effective at controlling the behaviour of the structure – Dinh *et al.* (2016) similarly used an STFT variable stiffness controller with a tight allowable band to control their turbine. The entire controller process is detailed in Fig. 8. An artificial 20 ms delay was inserted between calculating the target stiffness and implementing it to model the time required for the physical system to adjust.

$$w(t) = \sin^2\left(\frac{\pi t}{T}\right), \qquad t \in [0, T] \tag{23}$$

2.3.6 Parameter optimization

A trial-and-error parametric study was carried out to select the optimized values for the voltage range, window time, and stiffness limit coefficient of the TMD, based on the response of the TMD-equipped turbine tower subjected to fifteen random load cases (five each of the EQ, HIW, and SW load time histories). The averaged displacement and acceleration response of the turbine (which is fully detailed in Section 3) was used as the optimization index for the four parameters. Initial values of each parameter were estimated based on previous research, and the value of each parameter was individually studied in 0.05V, 0.5s, and 0.05 increments for the voltages, window times, and stiffness limit coefficient, respectively. The final combination of optimized parameter was confirmed to achieve superior results compared to all other tests performed during the parametric study. Some parameters of the STMDs were optimized on a per-load-type basis for increased effectiveness. The ability to change parameters based on the measured loading type is an advantage of a semi-active vibration control system, and could be achieved in reality using the existing equipment for wind speed measurement and an accelerometer at the base of the turbine (for EQ load cases). Table 8 lists the optimized parameters for the 3% modal mass ratio TMDs used in the final testing.

2.4 Numerical algorithm

The explicit Chen-Ricles (CR) numerical algorithm (Chen *et al.* 2009) was used in this testing, which is summarized in Eqs. (24) - (26). Here, j = 1 refers to the

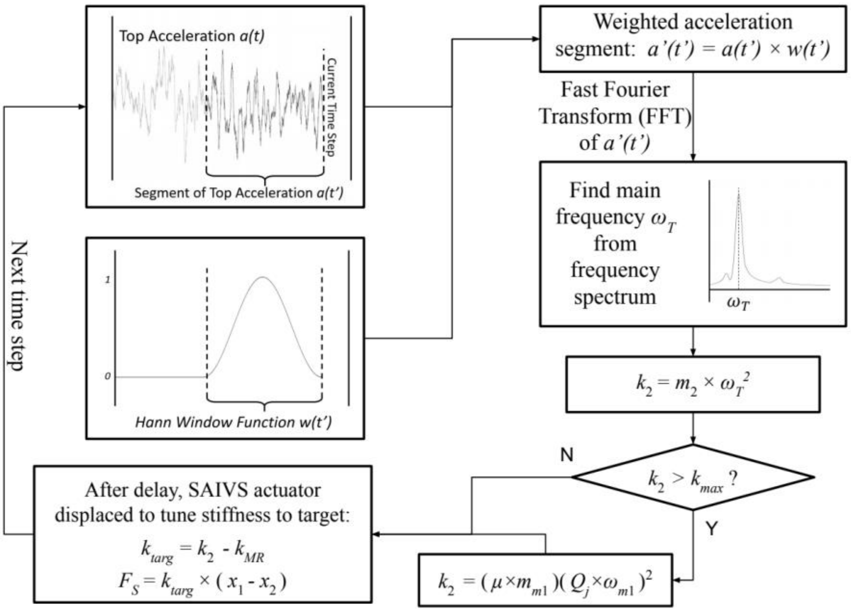

Fig. 8 Flowchart of a single time step of the VarS control process

Table 8 Optimized parameters for 3% modal mass ratio TMDs

Optimized parameters:	Load type:		
	EQ	HIW	SW
VarD: Maximum voltage v_{max} (V) [Eq. (20)]	3	1.5	0.75
VarD: Minimum voltage v_{min} (V) [Eq. (20)]		0	
VarS: Window time (s) [Fig. 8]		2	
VarS: Upper stiffness limit $k_{\max}$ (N/m) [Fig. 8]		$1.5 m_2 \omega_1{}^2$	

Algorithm 1 Numerical integration method for a simplified 2-DOF system

Input: F, K_1, K_2, C_1, C_2, M_1, M_2
Output: x_1, $\dot{x}_1$, $\ddot{x}_1$, x_2, $\dot{x}_2$, $\ddot{x}_2$
1. Calculate α_1, α_2 using Eq. (26)
2. For i = 2 to N
    3. Calculate $x_1(i)$, $\dot{x}_1(i)$ using Eqs. (24) - (25)
    4. Calculate $x_2(i)$, $\dot{x}_2(i)$ using Eqs. (24) - (25)
    5. Calculate F_D and F_S depending on TMD case – [see Section 2.3]
    6. Calculate $\ddot{x}_2(i)$ using TMD's equation of motion – Eq. (6)
    7. Calculate $\ddot{x}_1(i)$ using structure's equation of motion – Eq. (5)
8. End

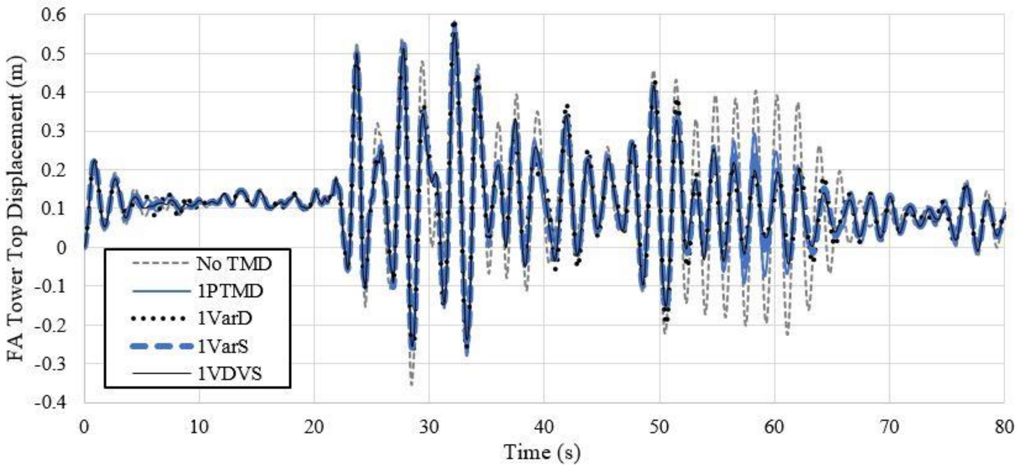

Fig. 9 Displacement time histories from EQ6 load case for single TMD cases

turbine and $j = 2$ refers to the TMD as in Fig. 6; i refers to the time step; x_j, $\dot{x}_j$, $\ddot{x}_j$ are the displacement, velocity and acceleration of the given mass; and Δt is the length of a time step in this analysis. α_j refers to the integration parameters for the CR algorithm, which is calculated using Eq. (26) where M_j, C_j, K_j refers to the mass, damping, and stiffness matrices of the given mass. In the MTMD cases, separate integration parameters were calculated for each TMD. In the semi-active cases where the stiffness and damping are not constant, approximate values were used in these calculations; the original authors (Chen *et al.* 2009) as well as testing here have found that the sensitivity of the integration parameter is very low, thus using these approximated values did not introduce notable error into the final results. Table 9 lists a summary of the stiffness and damping values used for each damper system (j = 2) for calculating the integration parameter. The CR algorithm was selected to accommodate possible future testing.

$$\dot{x}_{j,i+1} = \dot{x}_{j,i} + \Delta t * \alpha_j * \ddot{x}_{j,i} \tag{24}$$

$$x_{j,i+1} = x_{j,i} + \Delta t * \dot{x}_{j,i} + \Delta t^2 * \alpha_j * \ddot{x}_{j,i} \tag{25}$$

$$\alpha_j = \frac{4 * M_j}{4 * M_j + 2 * \Delta t * C_j + \Delta t^2 * K_j} \qquad j = 1,2 \tag{26}$$

Algorithm 1 details the full CR algorithm process used in this testing for a simplified 2-DOF system (using nomenclature from Fig. 6), where x_1, $\dot{x}_1$, and $\ddot{x}_1$ are the time histories of the displacement, velocity and acceleration responses of the main mass and x_2, $\dot{x}_2$, and $\ddot{x}_2$ are likewise for the TMD; N is the total number of time steps in the analysis; and F is the time history of the loading applied to the main mass.

3. Results of TMD comparisons

Each of the 121 load cases were applied to the uncontrolled wind turbine as well as turbines with the eight different TMD cases. Fig. 9 shows a selection of response time histories under EQ loading. The effectiveness of the various TMD systems were evaluated based on the FA and SS accelerations and displacements at the top of the turbine tower as well as at the maximum of the second mode of the structure where the lower TMD was placed, which are hereafter referred to as the Top and Mid points respectively. Since the TMDs only affect the fluctuating component of the response, the static component of the response was disregarded during analysis. The absolute mean of the displacements and accelerations over the entire 85 s time history were compared to find the improvement of the response due to the TMDs. This process for a given load case is summarized in Eqs. (27) - (28); n refers to the TMD case where the results of the uncontrolled turbine are 1 and the 1PTMD, 1VarD, 1VarS, 1VDVS, 2PTMD, 2VarD, 2VarS, and 2VDVS case results are 2 through 9 respectively; $\chi_n(:)$ is the entire time history of the response of interest – displacement or acceleration in the FA or SS directions at the Top or Mid point of the turbine; $\chi_{avg,n}$ is the absolute average mean of the fluctuating component used for comparison; $imp_{\chi_{avg,n}}$ is the percent improvement of the given TMD case compared to the uncontrolled turbine subjected to the same loading.

$$\chi_{avg,n} = mean\{\ |\chi_n(\ :\ ) - mean[\ \chi_n(\ :\ )]|\ \}, \qquad n = 1,2,\ldots,9 \tag{27}$$

$$imp_{\chi_{avg,n}} = \frac{(\chi_{avg,1} - \chi_{avg,n})}{\chi_{avg,1}}, \qquad n = 2,3,\ldots,9 \tag{28}$$

As both acceleration and displacement have been used as performance indices in previous testing [see Table 1], both were considered here. Acceleration is important to consider as the large inertial mass of the nacelle can cause large accelerations in the middle of the tower. The comparative improvements of each TMD case over the uncontrolled turbine for all the EQ, HIW, and SW load cases have been averaged and are shown in Tables 10-12. The eight response indices are averaged together across each TMD case to provide a broad comparison of the effectiveness of each TMD system, though this number may overvalue reductions in certain response indices depending on design goals.

These results clearly show that in all instances the addition of a TMD improved the response of the turbine compared to an uncontrolled turbine. The additional damping provided by the TMD had a much greater impact on controlling displacements in the SS direction where the structure lacked aerodynamic damping compared to the FA direction. Since the structure was parked in the HIW load cases and lacked aerodynamic damping, the TMDs were notably more effective in the FA direction here as well. In general, the TMDs were more effective at reducing the average displacement of turbines under HIW loading compared to EQ and SW loading.

The PTMD cases were shown to perform nearly as effectively as the semi-active cases. While the STMDs surpassed the PTMD in all cases, the difference in improvement of the average response reductions was only 2-3%. This difference was greatest when controlling the acceleration and displacement of the Mid point of the turbine, particularly in its single TMD configuration, compared to the most effective semi-active cases. The presence of realistic mechanical delays within the semi-active systems may play a part in why the mechanically-simpler PTMD performed so comparatively well.

The VarS system was overall the least effective semi-active controller, typically only showing a 0.51% difference in improvement in average response reduction compared to the PTMD. Due to the narrow tuning range of the VarS system, it was very effective at controlling the response of the top of the tower (generally surpassing the VarD case)

Table 10 Average percent improvement compared to uncontrolled turbine under EQ loading

μ = 3%	Displacement				Acceleration				Overall average
TMD case:	Fore-aft		Side-side		Fore-aft		Side-side		
	Top	Mid	Top	Mid	Top	Mid	Top	Mid	
1PTMD	9.6%	9.8%	33.4%	34.0%	9.7%	1.0%	25.7%	4.9%	16.0%
1VarD	9.0%	9.2%	34.8%	35.2%	11.2%	2.6%	28.5%	6.9%	17.2%
1VarS	9.2%	9.4%	35.2%	34.8%	12.2%	1.2%	29.5%	5.7%	17.1%
1VDVS	10.2%	10.3%	36.7%	37.0%	12.2%	2.9%	30.3%	7.1%	18.3%
2PTMD	8.2%	8.7%	32.3%	32.9%	11.6%	25.6%	26.1%	27.5%	21.8%
2VarD	8.4%	8.5%	34.9%	35.2%	13.0%	26.9%	29.4%	29.7%	23.3%
2VarS	9.4%	9.2%	35.1%	35.0%	13.3%	25.7%	30.8%	28.5%	23.2%
2VDVS	9.7%	10.0%	36.2%	36.5%	13.4%	26.9%	31.4%	29.6%	24.2%

Table 11 Average percent improvement compared to uncontrolled turbine under HIW loading

μ = 3%	Displacement				Acceleration				Overall average
TMD case:	Fore-aft		Side-side		Fore-aft		Side-side		
	Top	Mid	Top	Mid	Top	Mid	Top	Mid	
1PTMD	49.5%	49.7%	38.5%	37.5%	42.0%	2.5%	48.9%	3.9%	34.0%
1VarD	49.0%	50.4%	38.7%	37.7%	41.3%	5.5%	50.2%	6.2%	34.9%
1VarS	50.2%	49.2%	39.2%	38.1%	44.7%	2.5%	50.7%	4.0%	34.8%
1VDVS	51.0%	51.2%	38.9%	37.9%	44.8%	5.6%	51.4%	6.1%	35.9%
2PTMD	47.6%	47.9%	37.8%	36.8%	41.3%	10.7%	49.3%	20.1%	36.5%
2VarD	48.4%	48.9%	37.4%	36.5%	42.4%	14.0%	50.4%	22.7%	37.6%
2VarS	48.6%	48.7%	37.6%	37.3%	44.6%	10.7%	50.5%	20.2%	37.3%
2VDVS	49.3%	49.6%	38.3%	36.7%	44.9%	14.0%	51.1%	22.7%	38.3%

Table 12 Average percent improvement compared to uncontrolled turbine under SW loading

μ = 3%	Displacement				Acceleration				Overall average
TMD case:	Fore-aft		Side-side		Fore-aft		Side-side		
	Top	Mid	Top	Mid	Top	Mid	Top	Mid	
1PTMD	8.6%	8.6%	39.8%	40.3%	6.0%	0.4%	30.0%	2.2%	17.0%
1VarD	9.0%	9.1%	39.8%	41.1%	6.0%	1.8%	30.8%	4.0%	17.7%
1VarS	9.0%	9.1%	40.6%	40.3%	6.0%	0.4%	30.9%	2.3%	17.3%
1VDVS	9.2%	9.2%	41.9%	42.5%	6.6%	1.9%	31.5%	4.0%	18.3%
2PTMD	8.5%	8.6%	38.5%	39.0%	7.7%	19.8%	31.5%	20.3%	21.7%
2VarD	8.6%	8.9%	38.6%	40.5%	7.7%	21.5%	32.0%	22.3%	22.5%
2VarS	8.8%	8.7%	39.8%	39.1%	8.1%	19.8%	32.1%	20.4%	22.1%
2VDVS	8.8%	8.9%	41.2%	41.9%	8.6%	21.5%	33.1%	22.3%	23.3%

Table 13 Optimized parameters for 1.5% modal mass ratio TMDs

	Load type:		
Optimized parameters:	EQ	HIW	SW
VarD: Maximum voltage v_{max} (V) [Eq. (20)]	1.5	0.5	0.3
VarD: Minimum voltage v_{min} (V) [Eq. (20)]		0	
VarS: Window time (s) [Fig. 8]		2	
VarS: Upper stiffness limit $k_{\max}$ (N/m) [Fig. 8]		$1.5m_2{\omega_1}^2$	

Table 14 Average percent improvement of 1.5% mass ratio TMD compared to uncontrolled turbine

μ = 1.5%		Displacement				Acceleration				Overall average:
Load type:	TMD case:	Fore-aft		Side-side		Fore-aft		Side-side		
		Top	Mid	Top	Mid	Top	Mid	Top	Mid	
EQ	1PTMD	5.8%	5.9%	24.9%	25.5%	7.2%	0.7%	19.6%	3.6%	11.6%
	1VDVS	7.7%	7.9%	31.3%	31.5%	8.6%	2.0%	26.4%	6.0%	15.2%
HIW	1PTMD	36.1%	36.2%	32.8%	32.0%	33.8%	2.2%	40.6%	3.4%	27.1%
	1VDVS	42.4%	42.5%	35.3%	34.4%	36.4%	5.1%	45.3%	5.8%	30.9%
SW	1PTMD	6.5%	6.5%	35.0%	35.4%	4.4%	0.2%	26.2%	1.9%	14.5%
	1VDVS	6.7%	6.7%	37.1%	37.6%	5.2%	1.8%	28.4%	3.7%	15.9%

Table 15 Comparison of average improvement of 3% and 1.5% modal mass ratio TMDs vs uncontrolled turbine

	μ = 3%	μ = 1.5%			
Load type:	Av. reduction by 1PTMD	Av. reduction by 1PTMD	Ratio vs 3% 1PTMD	Av. reduction by 1VDVS	Ratio vs 3% 1PTMD
EQ	16.0%	11.6%	0.73	15.2%	0.95
HIW	34.0%	27.1%	0.80	30.9%	0.91
SW	17.0%	14.5%	0.85	15.9%	0.94
		Average:	0.79	Average:	0.93

but was less effective at controlling the Mid response of the tower – similar to the PTMD cases.

The VarD cases consistently reduced the turbine response compared to the PTMDs and VarS system, particularly when looking at the response of the Mid point of the tower where it was up to 4 times as effective as the PTMD and VarS cases, indicating that this system was more effective at controlling the second mode response of the structure which suggests a greater robustness compared to the narrowlytuned VarS cases. It suffered compared to the VarS cases at controlling the top of the tower, possibly due to the passive spring system not accounting for the additional stiffness provided by the MR damper in the varying-damper system.

The VDVS cases showed even further improvement in response reduction than the VarD and VarS cases – combining the varying-spring and varying-damper systems tended to result in improvements that were roughly cumulative of the improvements provided by the individual semi-active systems compared to the PTMDs; the improvement was slightly less than cumulative under EQ loading and slightly more under single-TMD SW loading. The VDVS controller was the most effective of all tested.

The introduction of the second passive TMD in the MTMD cases improved the overall average response reduction for all cases. The improvement was slightly larger under EQ loading (where the second mode of the structure was more heavily excited) and the SW loading (where the single TMDs were least effective at controlling the Mid response). It can be plainly seen that the MTMD systems were extremely effective at controlling the response of the Mid point of the tower – in some cases 50 times as effective – compared to the single TMD cases, though typically at the cost of a slight reduction of control of the top of the turbine tower.

To further analyze the advantages of the STMDs over the PTMDs, parameter optimization was performed (as per Section 2.3.6) for turbines equipped with 1.5% modal mass ratio TMDs (as opposed to the 3% mass ratio used above), which is summarized in Table 13. These new TMD-equipped turbines were subjected to the same 121 load cases; Table 14 lists the resulting average response improvement of a limited number of controlled turbines under the three loading types. It can be seen that, as before, the average reduction effect of the 1VDVS system surpasses the 1PTMD in all cases.

Table 15 compares the ratio of the average response reduction by the 1.5% modal mass ratio 1PTMD and 1VDVS systems from Table 14 to the average response reduction of the 3% modal mass ratio 1PTMD system from Tables 10-12. It can be seen that the response improvement provided by the 1.5% modal mass ratio 1VDVS damper is only slightly reduced (by about 7%) compared to the response reduction provided by the 3% modal mass ratio 1PTMD. Since a smaller TMD mass can result in a reduced P-delta effect on the tower, smaller space requirements, and simpler installation, it is a reasonable design goal to achieve the target response reduction with as small of a TMD mass as possible. This example shows that a notably lighter semi-active TMD can achieve a nearly equivalent response reduction effect compared to a heavier passive damping system.

4. Conclusions and recommendations

This paper presents a comparative study of eight tuned mass damper (TMD) systems used for vibration control of an onshore wind turbine subjected to service wind, high-intensity wind and seismic loading. A single passive TMD, three single semi-active TMDs (varying-spring, varying-damper, and varying-damper-and-spring), a passive multiple TMD (MTMD) system, and three mixed passive-and-semi-active MTMDs (where the upper TMD was semi-actively controlled using the three previous methods and the lower TMD was passive) were compared to an uncontrolled turbine. The design of these TMD systems were approached from a practical perspective using specific mechanical systems to achieve the variable properties and including realistic physical delays and limits. Overall, all the TMDs improved the response of the wind turbine, but the multiple semi-active varying-damper-and-spring TMD system (the 2VDVS case) was the most effective TMD case when considering all performance indices. The semi-active varying-damper (VarD) and varying-stiffness (VarS) systems also showed improved effectiveness compared to passive TMDs (PTMDs), with the former showing improved control of the middle of the tower and the latter showing improved control of the top of the tower. The use of a MTMD system with the same collective mass as a single TMD resulted in improved control of higher mode responses at the cost of a slight reduction in attenuation of the first mode. The improvement of the STMDs versus the PTMD cases was relatively small depending on the load case and index of interest, and must be weighed against the increased cost of implementing the semi-active systems, though in this specific case, a semi-active damper with half the mass was found to be almost equally effective as an optimized passive damper. Overall, the absolute best vibration reduction system will depend on the desired control for each performance index, the expected loading, and a cost-benefit analysis.

Future testing could build on this research by applyingthese dampers to a more widely-used wind turbine size such as NREL's standard 5MW wind turbine (Jonkman *et al.* 2009). Research could likewise be expanded by considering the effects of non-stochastic wind loads such as tornados (Gariola and Bitsuamlak 2019) or downbursts (Aboshosha *et al.* 2015a), potentially through the use of more robust simulation methods such as computational fluid dynamics (Dagnew and Bitsuamlak 2013). Results could be refined by employing more modern wind spectrum generation techniques, as the methods suggested in the IEC code (IEC 2005) have been found lacking in other research (Aboshosha *et al.* 2015b). Furthermore, it's possible that the controllers used here could be further improved which would directly impact the comparative effectiveness of the different semi-active systems.

The TMD system shown here to best balance simplicity and robustness was the single multi-directional TMD equipped with the varying-damper-and-spring system, which would be located at the top of the turbine tower below the nacelle with a braking system to allow maintenance workers to pass safely. Further study of this STMD using a more detailed FEM model as a practical vibration reduction system for controlling wind turbine vibrations is warranted.

Acknowledgments

The authors would like to acknowledge the support from the National Natural Science Foundation of China [grant numbers U1710111 & 51878426]; the International Collaboration Program of Sichuan Province [grant number 18GJHZ0111]; and the Fundamental Research Funds for Central Universities of China.

References

Aboshosha, H., Bitsuamlak, G. and El Damatty, A. (2015a), "Turbulence characterization of downburst using LES", *J. Wind Eng. Ind. Aerod.*, **136**, 44-61. https://doi.org/10.1016/j.jweia.2014.10.020.

Aboshosha, H., Elshaer, A., Bitsuamlak, G. and El Damatty, A. (2015b), "Consistent inflow turbulence generator for LES evaluation of wind-induced responses for tall buildings", *J. Wind Eng. Ind. Aerod.*, **142**, 198-216. https://doi.org/10.1016/j.jweia.2015.04.004.

Ancheta, T.D., Darragh, R.B., Stewart, J.P., Seyhan, E., Silva, W.J., Chiou, B.S.J., Wooddell, K.E., Graves, R.W., Kottke, A., Boore, D.M., Kishida, T. and Donahue, J. (2013), "PEER NGA-West2 Database", Pacific Earthquake Engineering Research Center, Berkeley, U.S.A.

Argyriadis, K. and Hille, N. (2004), "Determination of fatigue loading on a wind turbine with oil damping device", *In the Proceedings of the 2004 European Wind Energy Conference & Exhibition*, London.

Arrigan, J., Pakrashi, V., Basu, B. and Nagarajaiah, S. (2011), "Control of flapwise vibrations in wind turbine blades using semi-active tuned mass dampers", *J. Struct. Control Heal. Monit.*, **18**(8), 840-851. https://doi.org/10.1002/stc.404.

Asareh, M.A., Schonberg, W. and Volz, J. (2016), "Fragility analysis of a 5-MW NREL wind turbine considering aero-elastic and seismic interaction using finite element method", *Finite Elemen. Analy. Des.*, **120**(1), 57-67. https://doi.org/10.1016/j.finel.2016.06.006.

Brodersen, M.L., Bjorke, A. and Hogsberg, J. (2017), "Active tuned mass damper for damping of offshore wind turbine vibrations", *Wind Energy*, **20**(5), 783-796. https://doi.org/10.1002/we.2063.

Brodersen, M.L., Ou, G., Hogsberg, J. and Dyke, S. (2016), "Analysis of hybrid viscous damper by real time hybrid simulations", *Eng. Struct.*, **126**, 675-688. https://doi.org/10.1016/j.engstruct.2016.08.020.

Caterino, N. (2014), "Semi-active control of a wind turbine via magnetorheological dampers", *J. Sound Vib.*, **345**, 1-17. https://doi.org/10.1016/j.jsv.2015.01.022.

Caterino, N., Georgakis, C.T., Spizzuoco, M. and Occhiuzzi, A. (2016), "Design and calibration of a semi-active control logic to mitigate structural vibrations in wind turbines", *Smart Struct. Syst.*, **18**(1), 75-92. https://doi.org/10.12989/sss.2016.18.1.075.

Caterino, N., Georgakis, C.T., Trinchillo, F. and Occhiuzzi, A. (2014), "A semi-active control system for wind turbines", *Wind Turbine Control Monit.*, 375-407. https://doi.org/10.1007/978-3-319-08413-8_13.

Caterino, N., Spizzuoco, M. and Occhiuzzi, A. (2011), "Understanding and modelling the physical behaviour of magnetorheological dampers for seismic structural control", *Smart Mat. Struct.*, **20**(6). https://doi.org/10.1088/0964-1726/20/6/065013.

Caterino, N., Spizzuoco, M., and Occhiuzzi, A. (2013), "Promptness and dissipative capacity of MR dampers: Experimental investigations", Structural Control and Health Monitoring, 20, 1424-1440. https://doi.org/10.1002/stc.1578.

Chae, Y., Ricles, J.M. and Sause, R. (2012), "Modeling of a large-scale magneto-rheological damper for seismic hazard mitigation. Part 1: Passive mode", *Earthq. Eng. Struct. Dyn.*, **42**(5). https://doi.org/10.1002/eqe.2237.

Chen, C., Ricles, J.M., Marullo, T.M. and Mercan, O. (2009), "Real-time hybrid testing using the unconditionally stable explicit CR integration algorithm", *Earthq. Eng, Struct. Dyn.*, **38**(1), 23-44. https://doi.org/10.1002/eqe.838.

Chey, M., Chase, J.G., Mander, J.B. and Carr, A.J. (2009), "Semi-active tuned mass damper building systems: Design", *Earthq. Eng. Struct. Dyn.*, **39**(2), 119-139. https://doi.org/10.1002/eqe.934.

Chou, J.S. and Tu, W.T. (2011), "Failure analysis and risk management of a collapsed large wind turbine tower", *Eng. Fail. Analy*, **8**(1), 295-313. https://doi.org/10.1016/j.engfailanal.2010.09.008.

Chung, L., Lai, Y., Yang, C.W., Lien, K. and Wu, L. (2013), "Semi-active tuned mass dampers with phase control", *J. Sound Vib.*, **332**(15), 3610-3625. https://doi.org/10.1016/j.jsv.2013.02.008.

Connor, J.J. (2002), "Introduction to Structural Motion Control", Pearson.

Dagnew, A.K. and Bitsuamlak, G. (2013), "Computational evaluation of wind loads on buildings: a review", *Wind Struct.*, **16**(6), 629-660. https://doi.org/10.12989/was.2013.16.6.629.

Dai, K., Sheng, C., Zhao, Z., Yi, Z., Camara, A. and Bitsuamlak, G. (2017b), "Nonlinear response history analysis and collapse mode study of a wind turbine tower subjected to tropical cyclonic winds", *Wind Struct.*, **25**(1), 79-100. https://doi.org/10.12989/was.2017.25.1.079.

Dai, K., Wang, Y., Huang, Y., Zhu, W. and Xu, Y. (2017a), "Development of a modified stochastic subspace identification method for rapid structural assessment of in-service utility-scale wind turbine towers", *Wind Energy*, **20**(10), 1687-1710. https://doi.org/10.1002/we.2117.

Dai, K., Yichao, H., Changqing, G., Zhenhua, H. and Xiaosong, R. (2015), "Rapid seismic analysis methodology for in-service wind turbine towers", *Earthq. Eng. Eng. Vib*., **14**(3), 539-548. https://doi.org/10.1007/s11803-015-0043-0.

Diaz, O. and Suarez, L.E. (2014), "Seismic analysis of wind turbines", Earthq. Spectra, **30**(2), 743-765. https://doi.org/10.1193/123011EQS316M.

Dinh, V., Basu, B. and Nagarajaiah, S. (2016), "Semi-active control of vibrations of spar type floating offshore wind turbines", *Smart Struct*., **18**(4), 683-705. https://doi.org/10.12989/sss.2016.18.4.683.

Eason, R.P., Sun, C., Dick, A.J. and Nagarajaiah, S. (2013), "Attenuation of a linear oscillator using a nonlinear and a semi-active tuned mass damper in series", *J. Sound Vib*., **332**(1), 154-166. https://doi.org/10.1016/j.jsv.2012.07.048.

Esteki, K., Bagchi, A. and Sedaghati, R. (2011), "Semi-active tuned mass damper for seismic applications", Smart Materials Structures & NDT in Aerospace Conference, Montreal, Canada, November.

Gairola, A. and Bitsuamlak, G. (2019), "Numerical tornado modeling for common interpretation of experimental simulators", *J. Wind Eng. Ind. Aerod*., **186**, 32-48. https://doi.org/10.1016/j.jweia.2018.12.013.

Glauert, H. (1935), "Airplane Propellers", In Aerodynamic theory Springer, Berlin.

Global Wind Energy Council (2017), "Global Wind Statistics 2017", Brussels, Belgium. http://gwec.net/wp-content/uploads/vip/GWEC_PRstats2017_EN-003_FINAL.pdf.

Hartog, J.P.D. (1956), "Mechanical vibrations", McGraw-Hill.

He, E., Hu, Y. and Zhang, Y. (2017), "Optimization design of tuned mass dampers for vibration suppression of a barge-type offshore floating wind turbine", *J. Eng. Maritime Environ*., **231**(1), 302-315. https://doi.org/10.1177/1475090216642466.

Hemmati, A. and Oterkus, E. (2018), "Semi-active structural control of offshore wind turbines considering damage development", Journal of Marine Science and Engineering, 6(3), 102. https://doi.org/10.3390/jmse6030102.

Hrovat, D., Barak, P. and Rabins, M. (1983), "Semi-active versus passive or active tuned mass dampers for structural control", *J. Eng. Mech*., **109**(3), 691-705. https://doi.org/10.1061/(ASCE)0733-9399(1983)109:3(691).

Huang, C., Arrigan, J., Nagarajaiah, S. and Basu, B. (2010), "Semi-active algorithm for edgewise vibration control in floating wind turbine blades", *In Earth and Space 2010: Engineering, Science, Construction, and Operations in Challenging Environments.*

Hussan, M., Rahman, M.S., Sharmin, F., Kim, D. and Do, J. (2018), "Multiple tuned mass damper for multi-mode vibration reduction of offshore wind turbine under seismic excitation", *Ocean Eng*., **160**, 449-460. https://doi.org/10.1016/j.oceaneng.2018.04.041.

Hussan, M., Sharmin, F. and Kim, D. (2017), "Multiple tuned mass damper based vibration mitigation of offshore wind turbine considering soil-structure interaction", *Mech. Syst. Sig. Proc*., **105**, 338-360. https://doi.org/10.1016/j.ymssp.2017.12.011.

International Electrotechnical Commission (2005), "IEC 61400-1 International Standard: Wind turbines 3rd ed.", Geneva, Switzerland.

Jonkman, J. (2018), "FAST", National Renewable Energy Laboratory, Washington D.C. USA. https://nwtc.nrel.gov/FAST.

Jonkman, J., Butterfield, S., Musial, W. and Scott, G. (2009). "NREL/TP-500-38060: Definition of a 5-MW Reference Wind Turbine for Offshore System Development", Golden, U.S.A.

Katsanos, E., Thons, S. and Georgakis, C.T. (2016), "Wind turbines and seismic hazard: a state-of-the-art review", *J. Wind Energy*, **19**(11), 2113-2133. https://doi.org/10.1002/we.1968.

Kaveh, A., Pirgholizadeh, S. and Khademhosseini, O. (2015), "Semi-active tuned mass damper performance with optimized fuzzy controller using CSS algorithm", *Asian J. Civil Eng*., **16**(5), 587-606.

Kelly, N. and Jonkman, B. (2012), "TurbSim", National Renewable Energy Laboratory, Washington D.C. U.S.A.

Lackner, M.A. and Rotea, M.A. (2010), "Passive structural control offshore wind turbines", *J. Wind Energy*, **14**(3), 373-388. https://doi.org/10.1002/we.426.

Lackner, M.A. and Rotea, M.A. (2011), "Structural control of floating wind turbines", *J. Mechatronics*, **21**(4), 704-719. https://doi.org/10.1016/j.mechatronics.2010.11.007.

Li, X., Ozdagli, A.I., Dyke, S.J., Liu, X. and Christenson, R. (2017), "Development and verification of distributed real-time hybrid simulation methods", *J. Comput. Civil Eng*., **31**(4). https://doi.org/10.1061/(ASCE)CP.1943-5487.0000654.

Mardfekri, M. and Gardoni, P. (2015), "Multi-hazard reliability assessment of offshore wind turbines", *Wind Energy*, **18**(8), 1433-1450. https://doi.org/10.1002/we.1768.

Martynowicz, P. (2015), "Vibration control of wind turbine tower-nacelle model with magnetorheological tuned vibration absorber", *J. Vib. Control*, 1-22. https://doi.org/10.1177/1077546315591445.

Martynowicz, P. (2016), "Study of vibration control using laboratory test rig of wind turbine tower-nacelle system with MR damper based tuned vibration absorber", *Bull. Polish Academy Sci*., **64**(2). https://doi.org/10.1515/bpasts-2016-0040.

Martynowicz, P. (2017), "Control of a magnetorheological tuned vibration absorber for wind turbine application using the refined force tracking algorithm", *J. Low Freq. Noise, Vib. Active Control*, **36**(4), 339-353. https://doi.org/10.1177/1461348417744299.

Ministry of Housing and Urban-Rural Development of the People's Republic of China (2010), "Code for seismic design of buildings", Beijing, China.

Mo, R., Kang, H., Li, M. and Zhao, X. (2017), "Seismic fragility analysis of monopile offshore wind turbines under different operational conditions", *Energies*, **10**. https://doi.org/10.3390/en10071037.

Murtagh, P.J., Ghosh, A., Basu, B. and Broderick, B.M. (2008), "Passive control of wind turbine vibrations including blade/tower interaction and rotationally sampled turbulence", *Wind Energy*, **11**(4), 305-317. https://doi.org/10.1002/we.249.

Nagarajaiah, S. (2009), "Adaptive passive, semiactive, smart tuned mass dampers: identification and control using empirical mode decomposition, Hilbert transform, and short-term fourier transform", *J. Struct. Control Health Monit*., **16**(7), 800-841. https://doi.org/10.1002/stc.349.

Nagarajaiah, S. and Sonmez, E. (2007), "Structures with semiactive variable stiffness single/multiple tuned mass dampers", *J. Struct. Eng*., **133**(1), 67-77. https://doi.org/10.1061/(ASCE)0733-9445(2007)133:1(67).

Owji, H.R., Shirazi, A.H.N. and Sarvestani, H.H. (2011), "A comparison between a new semi-active tuned mass damper and an active tuned mass damper", *Procedia Eng*., **14**, 2779-2787. https://doi.org/10.1016/j.proeng.2011.07.350.

Park, S., Lackner, M.A., Cross-Whiter, J., Tsouroukdissian, A.R. and La Cava, W. (2016), "An investigation of passive and semi-active tuned mass dampers for a tension leg platform floating offshore wind turbine in ULS conditions", OMAE 2016 Proceedings, Busan, Korea, June.

Park, S., Lackner, M.A., Pourazarm, P., Tsouroukdissian, A.R.n and Cross-Whiter, J. (2019), "An investigation on the impacts of passive and semiactive structural control on a fixed bottom and a floating offshore wind turbine", *J. Wind Energy*, **22**, 1451-1471. https://doi.org/10.1002/we.2381.

Pinkaew, T. and Fujino, Y. (2001), "Effectiveness of semi-active tuned mass dampers under harmonic excitation", *Eng. Struct.*, **23**(7), 850-856. https://doi.org/10.1016/S0141-0296(00)00091-2.

Prowell, I., Veletzos, M., Elgamal, A. and Restrepo, J. (2009), "Experimental and numerical seismic response of a 65kW wind turbine", *J. Earthq. Eng.*, **13**(8), 1172-1190. https://doi.org/10.1080/13632460902898324.

Rahman, M., Ong, Z.C., Chong, W.T., Julai, S. and Khoo, S.Y. (2015), "Performance enhancement of wind turbine systems with vibration control: A review", *J. Renew. Sustain. Energy Rev.*, **51**, 43-54. https://doi.org/10.1016/j.rser.2015.05.078.

Reddy, J.N. (1993), "An introduction to the finite element method (2nd edition)", McGraw-Hill, Inc.

Rezaee, M. and Aly, A.M. (2016), "Vibration control in wind turbines for performance enhancement: A comparative study", *Wind Struct.*, **22**(1), 107-131. https://doi.org/10.12989/was.2016.22.1.107.

Ricciardelli, F., Occhiuzzi, A. and Clemente, P. (2000), "Semi-active tuned mass damper control strategy for wind excited structures", *J. Wind Eng. Ind. Aerod.*, **88**(1), 57-74. https://doi.org/10.1016/S0167-6105(00)00024-6.

Sadowski, A.J., Camara, A., Malaga-Chuquitaype, C. and Dai K. (2017), "Seismic analysis of a tall metal wind turbine support tower with realistic geometric imperfections", Wind Structures, **46**(2), 201-219. https://doi.org/10.1002/eqe.2785.

Spencer, B., Finholt, T.A., Foster, I., Kesselman, C., Beldica, C., Futrelle, J., Gullapalli, S., Hubbard, P., Liming, L., Marcusiu, D., Pearlman, L., Severance, C. and Yang, G. (2004), "NEESgrid: A Distributed Collaborator for Advanced Earthquake Engineering Experiment and Simulation", *The 13th World Conference on Earthquake Engineering*, Vancouver, Canada, August.

Stewart, G.M. (2012), "Load reduction of floating wind turbines using tuned mass dampers", Master Dissertation, University of Massachusetts Amherst, Amherst, U.S.A.

Sun, C. (2017), "Mitigation of offshore wind turbine responses under wind and wave loading: Considering soil effects and damage", *Struct. Control Health Monit.*, **25**(3). https://doi.org/10.1002/stc.2117.

Sun, C. and Jahangiri, V. (2018), "Bi-directional vibration control of offshore wind turbines using a 3D pendulum tuned mass damper", *Mech. Syst. Signal. Proc.*, **105**, 338-360. https://doi.org/10.1016/j.ymssp.2017.12.011.

Sun, C. and Nagarajaiah, S. (2013), "Study on semi-active tuned mass damper with variable damping and stiffness under seismic excitations", *J. Struct. Control Health Monit.*, **21**(6), 890-906. https://doi.org/10.1002/stc.1620.

Sun, C., Nagarajaiah, S. and Dick, A.J. (2014), "Experimental investigation of vibration attenuation using nonlinear tuned mass damper and pendulum tuned mass damper in parallel", J. Nonlinear Dyn., **78**(4), 2699-2715. https://doi.org/10.1007/s11071-014-1619-3.

Talatahari, S., Kaveh, A. and Mohajer Rahbari, N. (2012), "Parameter identification of Bouc-Wen model for MR fluid dampers using adaptive charged system search optimization", *J. Mech. Sci. Technol.*, **26**(8), 2523-2534. https://doi.org/10.1007/s12206-012-0625-y.

Tsouroukdissian, A.R., Park, S., Pourazarm, P., La Cava, W., Lackner, M., Lee, S. and Cross-Whiter, J. (2016), "Smart novel semi-active tuned mass damper for fixed-bottom and floating offshore wind", *Offshore Technology Conference*, Houston, U.S.A.

Valamanesh, V. and Myers, A.T. (2014), "Aerodynamic damping and seismic response of horizontal axis wind turbine towers", *J. Struct. Eng.*, **140**. https://doi.org/10.1061/(ASCE)ST.1943-541X.0001018.

Veers, P.S. (1988), "Three-dimensional wind simulation", Sandia National Laboratories, Albuquerque, U.S.A.

Wang, Z., Zhao, Y., Li, F. and Jiang, J. (2013), "Extreme dynamic responses of MW-level wind turbine tower in the strong typhoon considering wind-rain loads", *Math. Probl. Eng.*, **2013**. https://doi.org/10.1155/2013/512530.

Yang, G., Spencer, B.F., Carlson, J.D. and Sain, M.K. (2002), "Large-scale MR fluid dampers: modeling and dynamic performance considerations", *Eng. Struct.*, **24**, 309-323. https://doi.org/10.1016/S0141-0296(01)00097-9.

Zhang, R., Zhao, Z. and Dai, K. (2019), "Seismic response mitigation of a wind turbine tower using a tuned parallel inerter mass system", *Eng. Struct.*, **180**, 29-39. https://doi.org/10.1016/j.engstruct.2018.11.020.

Zhao, Z., Dai, K., Camara, A., Bitsuamlak, G. and Sheng, C. (2019a), "Wind turbine tower failure modes under seismic and wind loads", *J. Perform. Construct. Facil.*, **33**(2). https://doi.org/10.1061/(ASCE)CF.1943-5509.0001279.

Zhao, Z., Dai, K., Lalonde, E.R., Meng, J., Li, B., Ding, Z. and Bitsuamlak, G. (2019b), "Studies on application of scissor-jack braced viscous damper system in wind turbines under seismic and wind loads", *Eng. Struct.*, **196**. https://doi.org/10.1016/j.engstruct.2019.109294.

Zuo, H., Bi, K. and Hao, H. (2017), "Using multiple tuned mass dampers to control offshore wind turbine vibrations under multiple hazards", *Eng. Struct.*, **141**(15), 303-315. https://doi.org/10.1016/j.engstruct.2017.03.006.

FR